Earth, Planets and Space

FULL PAPER Open Access

Rheological properties of halloysite soil slurry: a case study of weathered tephra involved in a shallow landslide triggered by the 2018 Eastern Iburi earthquake in Hokkaido, Japan

Jun Kameda*

Abstract

The 6.7 M_w Eastern Iburi earthquake of 6 September 2018 triggered destructive landslides in southern Hokkaido, Japan, many of which were characterized by the flow-like downslope movement of volcanic soils formed from weathered tephra containing halloysite. This study aims to elucidate the mechanism of landslide generation through rheological characterization of halloysite soil slurries. The examined slurries were prepared from either oven-dried or moist soil. Both slurries showed a power-law correlation between measured yield stress and moisture content. However, at a given water content, slurry made from dried soil showed stresses that are one-to-two orders of magnitude lower than those of slurry made from moist soil. Compared with the measurements for the slurry of dried soil, those for the slurry of moist soil are closer to prior numerical modeling of a specific landslide, indicating that the soils involved were moist. The yield stress also varied with slurry pH, generally increasing with decreasing pH, which is in part explained by the DLVO force model based on the electrical double layer and van der Waals forces between the colloidal particles. The pH dependence is more prominent in the slurry of moist soil, and thus the mechanical state of the slope appears to vary significantly with rainfall-induced changes in subsurface chemistry. Dynamic viscoelasticity measurement indicated that both initially solid-like slurries can become fluid under an applied oscillatory strain of 0.5 to 10 Hz: the susceptibility to fluidization depends greatly on water content and frequency. The ground motion during the earthquake easily fluidized the slurry, indicating this was a factor contributing to the observed flow-like landslides.

Keywords: 2018 Hokkaido Eastern Iburi earthquake, Shallow landslide, Rheology, Slurry, Halloysite

*Correspondence: kameda@sci.hokudai.ac.jp
Department of Earth and Planetary Sciences, Faculty of Science, Hokkaido University, N10W8, Kita-ku, Sapporo 060-0810, Japan

Graphical Abstract

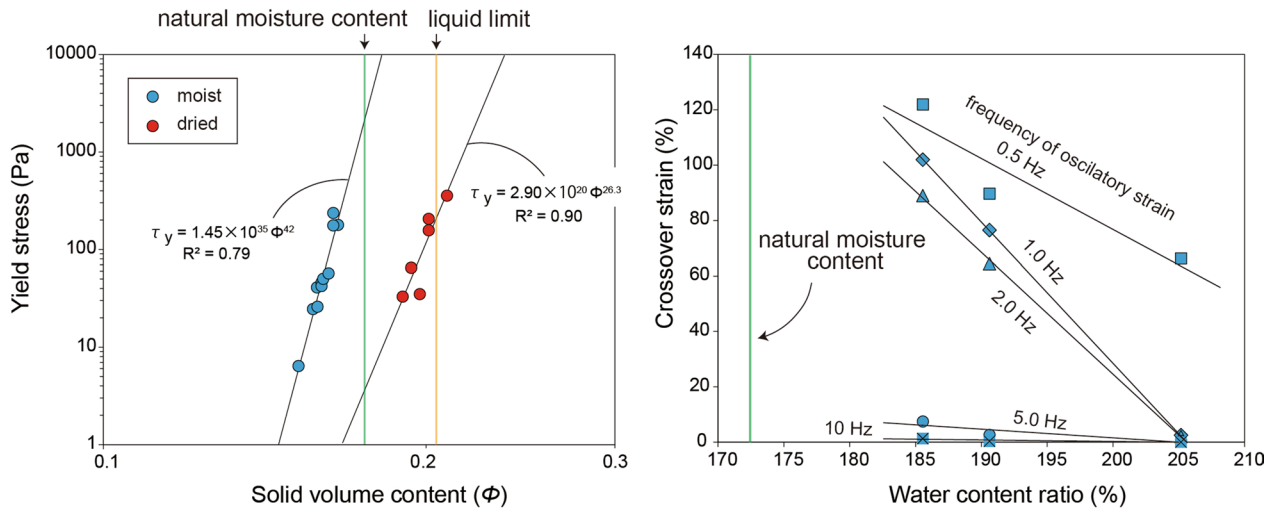

Introduction

Halloysite is a common weathering product of pyroclastic fall deposits and is often found on the failure surfaces of landslides in volcanic areas (Moon 2016). A recent example is the destructive landslides triggered by the Eastern Iburi earthquake ($M_w = 6.7$) that occurred at 3:07 A.M. (local time) on 6 September 2018 in southern Hokkaido, Japan (Fig. 1a). The strong ground motion (with a maximum intensity of 7 on the Japan Meteorology Agency [JMA] intensity scale) caused the sudden collapse of hill slopes that are widely covered by volcanic soils near the epicenter (Yamagishi and Yamazaki 2018; Osanai et al. 2019). These soils were formed by the weathering of pyroclastic deposits from Tarumae, Eniwa, and Shikotsu volcanoes. Most of the shallow landslides exhibited flow-like slope failures characterized by long travel distances along relatively gentle slopes (< 30°; Kasai and Yamada 2019; Osanai et al. 2019; Zhang et al. 2019). A field survey of one of the shallow landslides in Atsuma town (Fig. 1a, b) observed the slip surface at the base of a tephra erupted from Tarumae volcano (Ta-d) (Fig. 1c; Kameda et al. 2019). The survey found the basal part of Ta-d, including the slip surface, to be clayey and generally wet, and XRD analysis identified halloysite as a principal clay mineral (Kameda et al. 2019; Kameda 2021). Halloysite was also found in the equivalent horizon at other locations (Chigira et al. 2019; Ito et al. 2020). Quantitative analyses revealed halloysite contents of up to 40% (Kameda 2021).

Halloysite is a 1:1 dioctahedral clay mineral with a structure and chemical composition very similar to kaolin, except that it commonly contains water molecules between its layers (Joussein et al. 2005). It exhibits various morphological features, such as spheroidal, platy, tubular, or irregular shapes, but short and/or long tubes are most common in nature. Microscopic observation in the study area found halloysite with an irregular to spherical morphology (Kameda 2021). Other studies, however, have found halloysite with particles shaped like wood shavings (Wada and Mizota 1979) or thin plates (Earthquake and Volcano Hazards Observation and Research Program 2019). This indicates that halloysite's morphology possibly depends on location, even within a given stratum, but in general, tubular halloysite seems to be rare in the present study area. The mechanical and rheological properties of halloysite or halloysite soil depend on halloysite morphology (Moon 2016). Spherical halloysite generally has lower peak and remoulded strengths than the other morphologies (Kluger et al. 2017). Tubular halloysite exhibits higher peak and residual friction angles, possibly due to its limited ability to develop a preferred orientation (Moon 2016). Rheological tests of slurries containing halloysite of different morphologies have demonstrated that spherical halloysite gives a lower yield stress and viscosity than platy or tubular halloysite (Theng and Wells 1995). Considering these results, the formation of non-tubular halloysite in the study area may have contributed to the occurrence of flow-like slope failures. The above experiments revealed that, in addition to morphology, factors such as solid concentration and chemical conditions greatly affect the rheological properties of slurry. The rheological properties of many other clay minerals

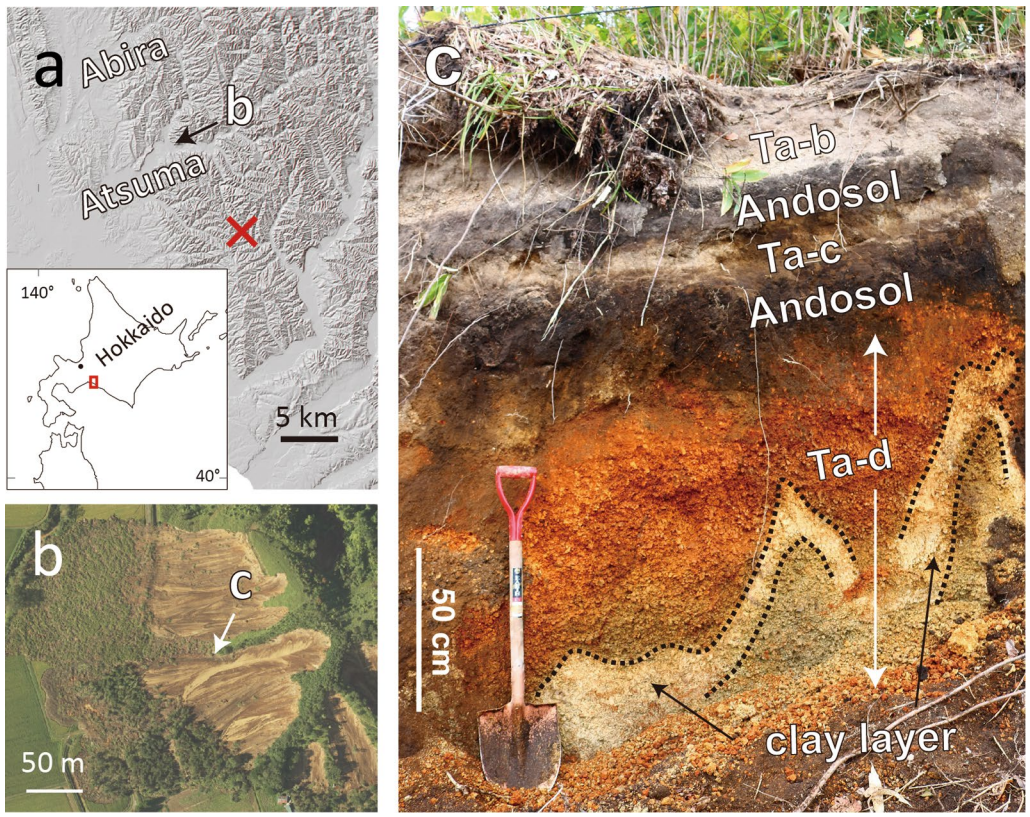

Fig. 1 **a** Locations of the epicenter of the Eastern Iburi earthquake (red cross) and the studied landslide in the Tomisato district (42.762°N, 141.931°E; black arrow). **b** Aerial view of the landslide (Geospatial Information Authority of Japan, 2018). **c** Lateral scarp showing a stratigraphic sequence of volcanoclastic deposits from Tarumae volcano (modified after Kameda et al. 2019). Weathered tephra samples were collected from the clay layer in the Ta-d layer that is in contact with the underlying Neogene sedimentary rock. The clay layer contains 40% halloysite (Kameda 2021)

(e.g., bentonite, kaolin, and mica) are known to depend on various factors, including slurry pH (Au et al. 2014; Au and Leong 2016), and studies have sought to understand the behaviors in terms of the surface properties of particles comprising the slurry. Although some mechanical tests in the field and laboratory have examined the relevant materials (Li et al. 2020; Wang et al. 2021), the dependence of rheological properties on moisture content and chemical conditions remains to be fully elucidated. Kameda (2021) discussed the possibility of rainfall-induced changes in the chemical state of pore water, which could in turn affect the mechanical properties of soils when the landslides occurred.

This work reports the results of rheological experiments on slurries of tephra sampled from the area of a landslide induced by the 2018 Hokkaido Eastern Iburi Earthquake, and attempts to ascertain the mechanical state of the slope when failure occurred. In addition to the effects of moisture content and chemical composition (slurry pH), dynamic viscoelasticity was tested to investigate the effect of cyclic strain caused by seismic motion. A mechanism of landslide occurrence is discussed based on the results.

Samples and methods

Samples

Soil samples containing halloysite were collected from the scarp of the landslide in 2018 and 2019 ("clay layer" in Fig. 1c). Based on field observations as well as the results of laboratory measurements, this clay layer was in most cases found to act as a slip surface during the landslide (Kameda et al. 2019). They were stored in a bucket covered with plastic to prevent drying. The bulk sample was sieved by straining with a rubber spatula to prepare slurries with particles < 425 μm, which is equivalent to the size fraction for soil mechanical testing. As the material properties of soil vary with heating and drying (e.g., Terzaghi et al. 1996; Sunil and Krishnappa 2012; Huvaj and Uyeturk 2018), two types of slurry were examined: one prepared from soil dried at 40 ℃ in an oven (water content of 5.2 wt%), and another made using moist soil that was not allowed to dry between sampling and slurry

preparation. The dried and moist soil samples were dispersed in pure water at different solid/water ratios, and were homogenized using a laboratory mixer. To account for moisture in both soil samples when determining the slurries' solid/water ratios, part of each was further dried at 110 ℃ to measure the dry mass and (residual) moisture content. The natural pH of the slurries was 6–7. When testing the effect of pH on mechanical properties, an appropriate amount of concentrated NaOH or HNO_3 solution was added to prepare the desired pH and solid/water ratio.

Rheological experiments

Yield stress measurement by the vane method

The yield stress of each slurry was measured using a viscometer (DV2T, Brookfield) with a four-blade vane spindle (Fig. 2). This technique measures the static yield stress at single point, and has been used for a variety of clay slurries, such as bentonite and kaolin (Nguyen and Boger 1983; Shankar et al. 2010; Au et al. 2014; Huang et al. 2016). The maximum torque reading T_m (N·m) was converted to yield stress τ_y (Pa) as follows (Nguyen and Boger 1983):

$$T_m = \frac{\pi D^3}{2}\left(\frac{H}{D}+\frac{1}{3}\right)\tau_y, \tag{1}$$

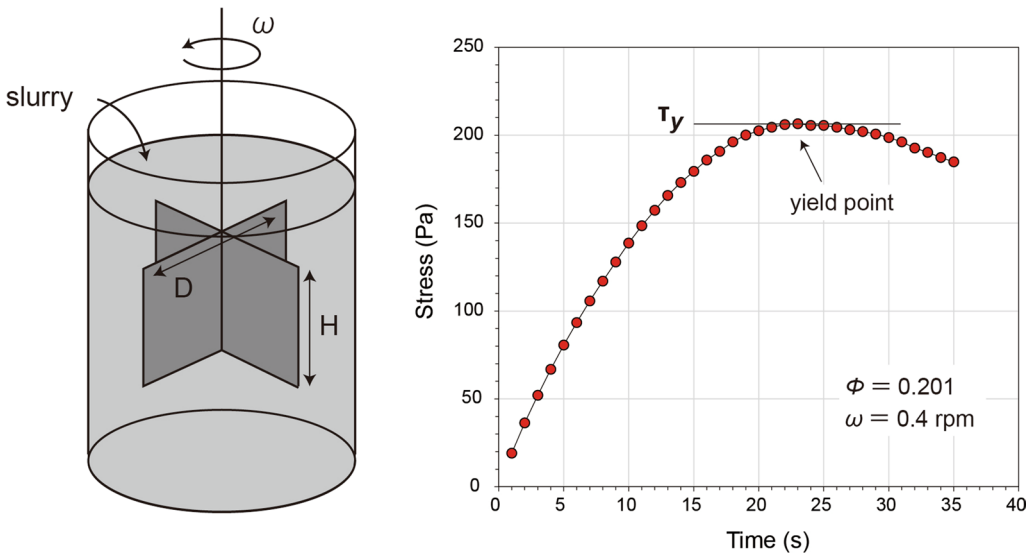

Fig. 2 Schematic image of vane measurement (left) and example measurement results for slurry made of dried soil (solid volumetric fraction $\varphi = 0.201$; right). The vane spindle was rotated at 0.4 rpm during measurement

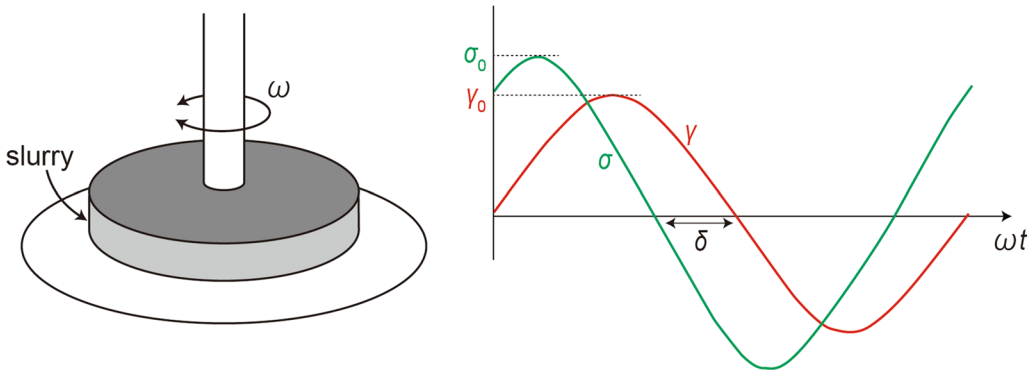

Fig. 3 Schematic image of dynamic viscoelasticity measurement (left) and strain/stress relationship (right)

where D and H are the vane diameter and height (m), respectively. The vane was rotated at 0.4 rpm, as the yield stress of flocculated suspensions has been shown to be independent of rotational speed in the range from 0.1 to 8 rpm (Nguyen and Boger 1983). After rotating at a constant speed, the torque at that time is recorded every second (Fig. 2). Due to the torque limitation of the viscometer, the range of stress that can be measured under the present conditions is < ~ 500 Pa.

After resting (normally 12 h for slurry of dried soil, as described below), the slurry was again stirred prior to yield stress measurement by the laboratory mixer. This ensured that the measurements were performed on a completely broken-down slurry (Goh et al. 2011). Structural recovery from this state was not characterized in this study.

Dynamic viscoelasticity measurement

Dynamic viscoelasticity testing (strain sweep testing) was conducted using an HR-2 rheometer (TA Instruments) with a parallel-plate geometry (Fig. 3). The rheometer contained an aluminum rotational upper plate with a diameter of 60 mm and a stationary lower Peltier plate kept at 20 °C. To avoid the influence of wall slip (i.e., slip between the slurry and the adjacent metal plate, rather than within the slurry), which is a common problem during rheometric experiments, waterproof sandpaper ($\phi = 125$ μm) was attached to the upper plate. Slurry samples were loaded into the 3.0-mm gap between the upper and lower plates.

Strain sweep tests were conducted by applying oscillatory shear strain ($\gamma(t) = \gamma_0 \cos(\omega t)$) with amplitude γ_0 increasing from 0.01% to 100% at a constant frequency (0.5, 1.0, 2.0, 5.0, and 10 Hz). Cyclic triaxial tests commonly employ a frequency of 1.0 Hz when measuring the resistance of soils to liquefaction (ASTM Standard D5311 2011). The stress under the above oscillatory strain can be expressed as

$$\sigma(t) = \sigma_0 \cos(\omega t - \delta) = \gamma_0 \left[G'(\omega)\cos(\omega t) - G''(\omega)\sin(\omega t) \right], \quad (2)$$

where G' ($= \frac{\sigma_0}{\gamma_0}\cos\delta$) and G'' ($= \frac{\sigma_0}{\gamma_0}\sin\delta$) are termed the frequency-dependent storage and loss-modulus, respectively, and δ is the phase difference between the strain and stress (Barnes et al. 1989; Fig. 3). The solid-to-liquid phase transition was determined from the crossover point between G' and G'', where δ was 45° (i.e., $\tan\delta = 1$). All strain sweep tests were performed immediately after sample loading without pre-shearing.

Zeta potential analysis

The zeta potential of the clay-size fraction (< 2 μm) of the same tephra sample has previously been determined (Kameda 2021). As the present rheological experiment used a different size fraction (i.e., < 425 μm), the zeta potential was remeasured for each sample. In accordance with previous studies that measured various clay samples (e.g., Au et al. 2014; Au and Leong 2016), the solid concentration of the slurries was diluted to about 1 wt% in the present measurements (with a solid concentration of 1.56 wt% dried soil or 0.99 wt% moist soil). The slurries were first adjusted to pH ~ 13 by adding concentrated NaOH solution and were then gradually acidified (by approximately 0.5 pH unit) by adding nitric acid solutions (0.6 N, 0.1 N, and 0.06 N). The zeta potential was measured at each condition.

The electrophoretic mobility μ of each sample was measured by electrophoretic light scattering with Zetasizer Nano (Malvern), and the zeta potential ζ was obtained as follows based on the Smoluchowski relationship (Smoluchowski 1921):

$$\mu = \frac{\varepsilon_0 \varepsilon \zeta}{\eta}, \quad (3)$$

where ε_0 is the vacuum permittivity, ε is the dielectric constant of water, and η is the viscosity of the solution.

Results

Figure 4 shows the change of yield stress over time for the slurry of dried soil (solid concentrations of 41.8 and 40.6 wt%; Additional file 1: Table S1). Slurry with higher solid concentrations exhibited a higher yield stress, but the stress of the two slurries quickly dropped by about half (from 650 to 350 Pa over 400 min for the 41.8 wt% slurry and from 500 to 250 Pa over 200 min for the 40.6 wt% slurry), before remaining relatively stable for

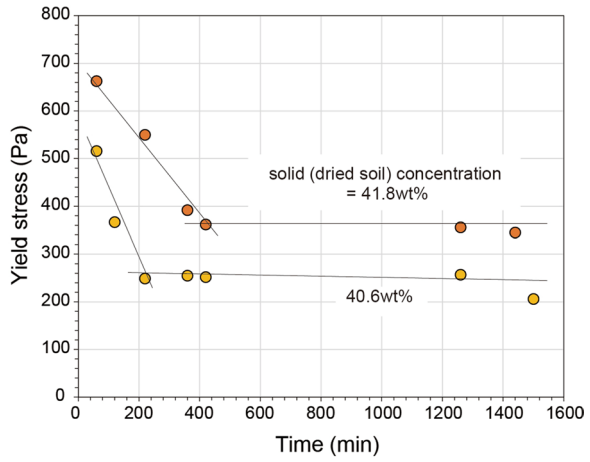

Fig. 4 Temporal evolution of yield stress for slurry of dried soil (solid concentrations of 41.8 and 40.6 wt%). The yield stress decreased rapidly in the first few hours and then remained constant

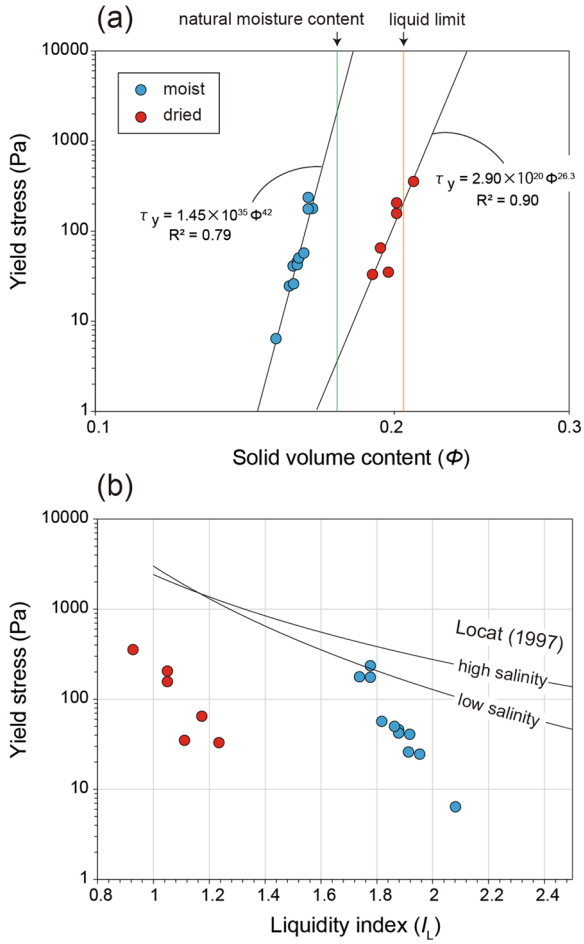

Fig. 5 **a** Yield stress versus solid volume content for slurries of moist (blue) and dried (red) soil with power-law fittings. **b** Yield stress versus liquidity index of each slurry. Empirical relations for several types of clay slurry are also shown (Locat 1997)

Table 1 Mechanical properties of the analyzed soil sample (Kameda et al., 2019)

Natural moisture content ratio w (%)	172
Liquid limit w_L (%)	143.3
Plastic limit w_P (%)	86.1
Plasticity Index I_P	57.2
Liquidity Index I_L (at natural moisture state)	1.51
Grain density ρ_S (g/cm^3)	2.719

the remainder of the 24 h test. Owing to these finding, all subsequent tests of this type of slurry involved standing the slurry for 12 h after preparation before taking measurements.

Figure 5a shows the correlation between yield stress and solid volumetric concentration (ϕ) for the two types of slurry (ϕ is estimated from the grain density of the sample (2.719 g/cm^3); Table 1). The properties of the slurry strongly depend on whether the soil samples were dried. The limitation of the apparatus's torque prevented testing of these slurries with equivalent ϕ ranges. For a given ϕ, the yield stress of the slurry with moist soil was several orders of magnitude larger than that of the other slurry. For each series of samples, the correlation almost follows a power law function, which has also been observed for flocculated clay suspensions (e.g., Au and Leong 2016; Kameda and Hamada 2021) and debris materials involved in landslides (Malet et al. 2004; Scotto di Santolo et al. 2010). Figure 5a also shows the liquidity limit and natural moisture content ratio of each sample from a previous study (Kameda et al. 2019). Extrapolation of the two power law curves indicates that the yield stress of the slurry of dried soil was several pascal at the natural moisture state, whereas that of the slurry of moist soil was as high as 2.2 kPa.

Figure 5b shows the yield stress with respect to the liquidity index (I_L) of each slurry, which was calculated from the sample's liquid limit and plastic limit (Table 1). The figure also shows empirical relations between the two parameters for a wide range of clay slurries, as represented by the following equations (for low- and high-salinity (0 and 30 g/L) cases, respectively; Locat 1997; Jeong et al. 2010):

$$\tau_y = \left(\frac{5.81}{I_L}\right)^{4.55}, \tag{4}$$

$$\tau_y = \left(\frac{12.05}{I_L}\right)^{3.13}. \tag{5}$$

The slurry of dried soil showed stress values one-to-two orders of magnitudes smaller than those from the empirical curves. For the slurry of moist soil, the plot of highest stress is close to the empirical curves (Eqs. 4 and 5), but the stress gradually deviates downward with increasing I_L.

Figure 6a shows the pH dependence of yield stress (for solid concentrations of 40.6 wt% dried soil and 34.8 wt% moist soil), with stress steadily increasing with decreasing pH. The slurry of dried soil showed a relatively moderate increase in stress from less than 100 Pa at pH 8.5 to 450 Pa at pH 5; the slurry of moist soil showed an initial gradual increase in stress from 5 Pa at pH 7.5 to 50 Pa at pH 6.4, and then a rapid increase to more than 500 Pa (the upper torque limit of the apparatus) at pH 5.7.

Figure 6b shows electrophoresis results for slurries with solid concentrations of 1.56 wt% dried soil and

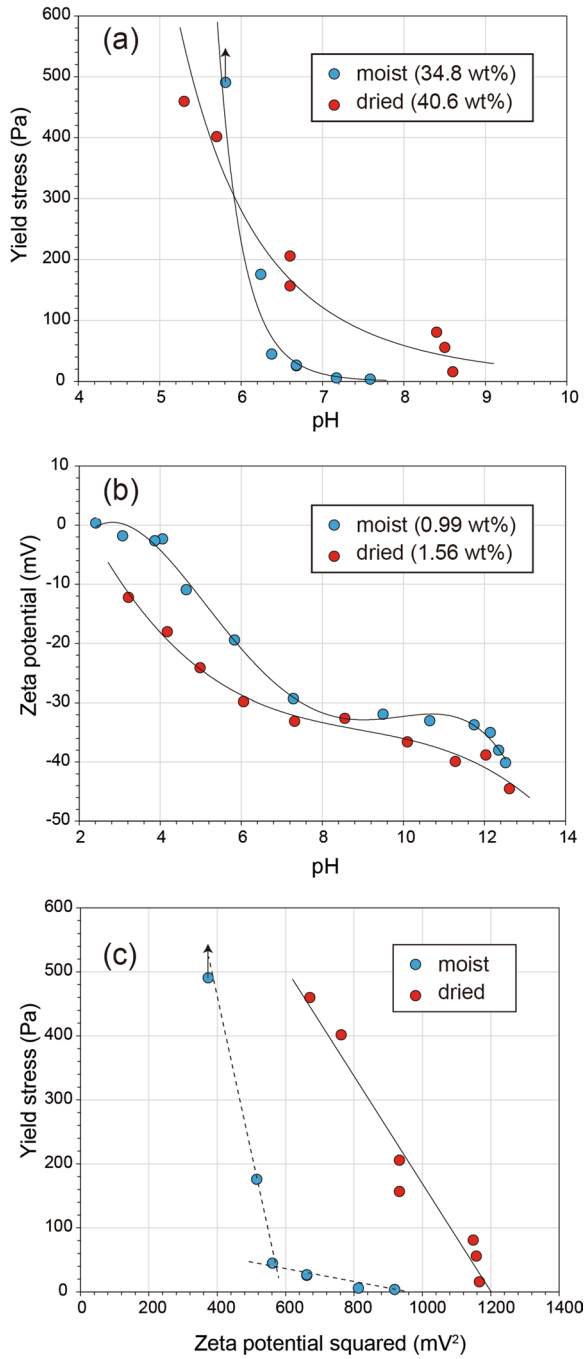

Fig. 6 **a** Yield stress versus pH for slurry with a fixed solid concentration of 34.8 wt% moist soil (blue) or 40.6 wt% dried soil (red). **b** Zeta potential with respect to pH: slurry with 0.99 wt% moist soil (blue) or 1.56 wt% dried soil (red). **c** Yield stress versus zeta potential squared. The zeta potential at each pH is derived from a polynomial fit of the zeta potential data in **b**

0.99 wt% moist soil. Similar to the yield stress variation (Fig. 5a), the zeta potential generally increased with decreasing pH. For the slurry of dried soil, the potential increased from − 45 mV at pH ~ 12 to − 13 mV at pH ~ 3. The measured zeta potential was roughly consistent with values previously obtained for a smaller size fraction (< 2 μm): − 40 to − 35 mV at pH 10, increasing to − 10 mV at pH 2 (Kameda 2021). The potential of the slurry of moist soil tended to increase more steeply as pH changed from neutral to acidic than did that of the other slurry.

Figure 6c shows the correlation between the yield stress and the square of zeta potential at each pH condition, which was derived from a polynomial fit of the zeta potential data (Fig. 6b). Both slurries show generally decreasing yield stress with increasing square of the zeta potential: the data for the slurry of dried soil show an almost linear correlation, while those for the slurry of moist soil do not clearly fit a linear trend.

Figure 7a–c shows the results of oscillatory strain sweep testing at a frequency of 1.0 Hz for slurries of 39.3, 38.6, and 37.7 wt% solid concentration of dried soil, respectively (Table S2). With increasing strain amplitude, both G' and G'' decreased steadily, while tan δ rapidly increased after initially remaining constant. The solid-to-fluid phase transition, where G' and G'' crossover (or equivalently, where tan $\delta = 1$), shifted to smaller amplitudes (in order 15%, 13%, 6%) with decreasing solid concentration. Figure 7d summarizes the results and shows the correlation between the strain of the fluidizing point (crossover strain) and the water content at different frequencies. The strain decreased steadily with increasing water content at a given frequency. Higher frequency resulted in a smaller amplitude for the solid-to-fluid transition. Under the natural moisture state ($w = 172\%$; Table 1), the slurry is expected to be easily fluidized by a small amplitude of shear strain oscillating at 1.0 Hz or more.

Figure 8a–c shows the results of oscillatory strain sweep testing at a fixed solid concentration (34.8 wt% for the slurry of moist soil), but under variable frequency (0.5, 1.0, and 10 Hz). The solid-to-fluid transition point steadily shifted to smaller amplitude (from ~ 100% to ~ 1%) with increasing oscillation frequency. Figure 8d summarizes the results and shows the correlation between the strain of the fluidizing point and the water content ratio at different frequencies. Similarly to the results for the slurry of dried soil, the strain generally decreased steadily with increasing

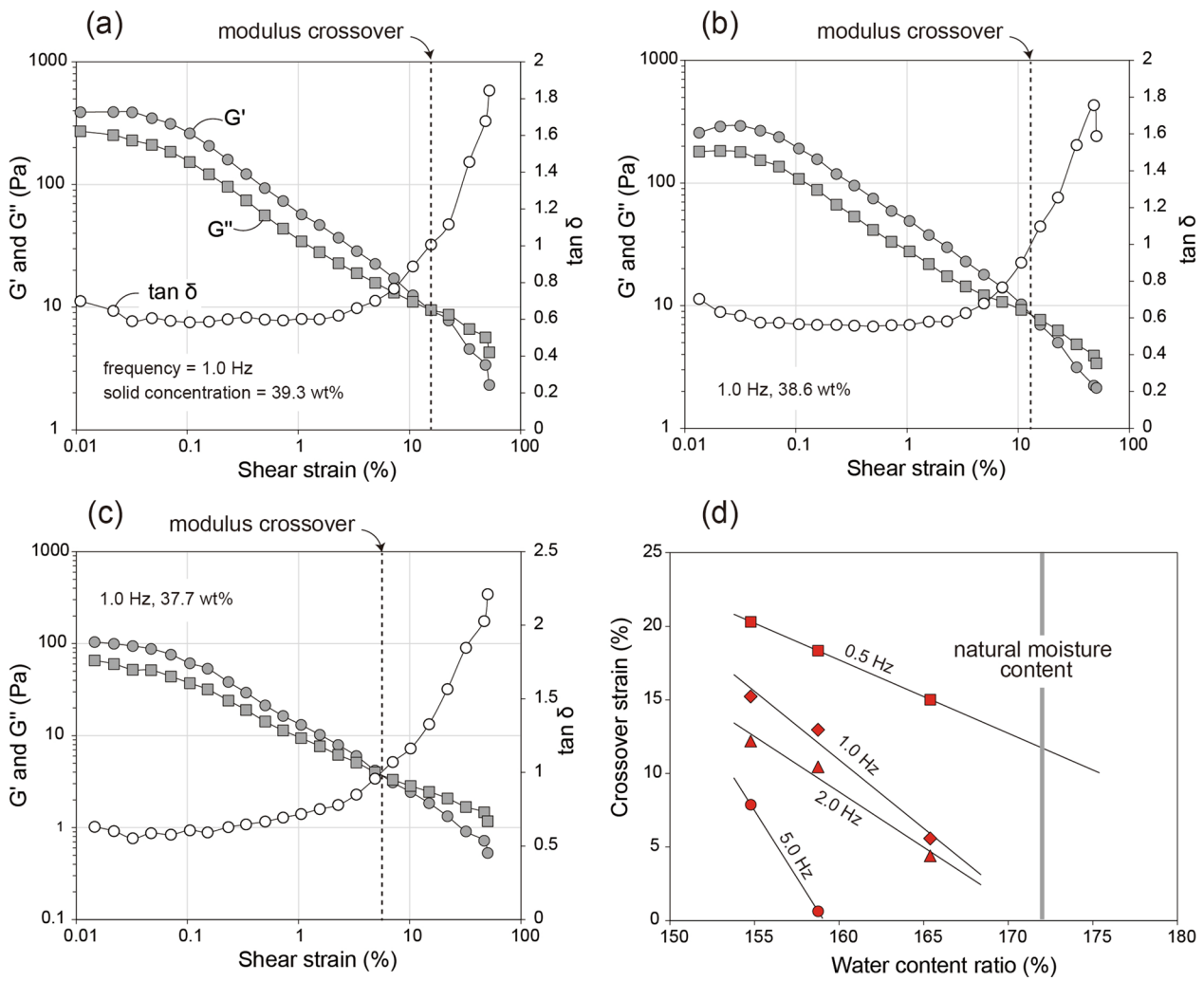

Fig. 7 (a–c) G', G'', and tan δ of slurry of dried soil with respect to shear strain at a fixed frequency of 1.0 Hz with solid concentrations of **a** 39.3, **b** 38.6, and **c** 37.7 wt%. Modulus crossover (where the magnitudes of G' and G'' are reversed) represents the solid-to-liquid transition. The crossover strain decreased with decreasing solid concentration (i.e., increasing water content). **d** Summary of the crossover strain for each frequency with respect to water content. Natural moisture content is also shown

water content at a given frequency. However, the range of water contents tested was higher than for the slurry of dried soil by $w = \sim 40$ wt%. Higher frequency led to a smaller amplitude for the solid-to-fluid transition. When the applied frequency was 5.0 Hz or higher, the strain remained relatively small (10% or less within the test range); however, strain greatly increased to at least 100% when the frequency was less than 2.0 Hz. Under natural moisture conditions, the sample's resistance to fluidization depends on whether the frequency of oscillatory strain is more than 2–5 Hz.

Discussion

Difference in yielding behaviors of slurries formed from dried and moist soil

The present experiments revealed that the yielding and fluidization behavior of slurries of weathered tephra depend greatly on several factors. As mentioned above, the yield stress is greatly affected by the slurry's water content; despite this, comparison with the liquidity index shows that the yield stresses of both types of slurry are generally lower than those expected from empirical relations (Fig. 5b). One reason for this is that the yield stress

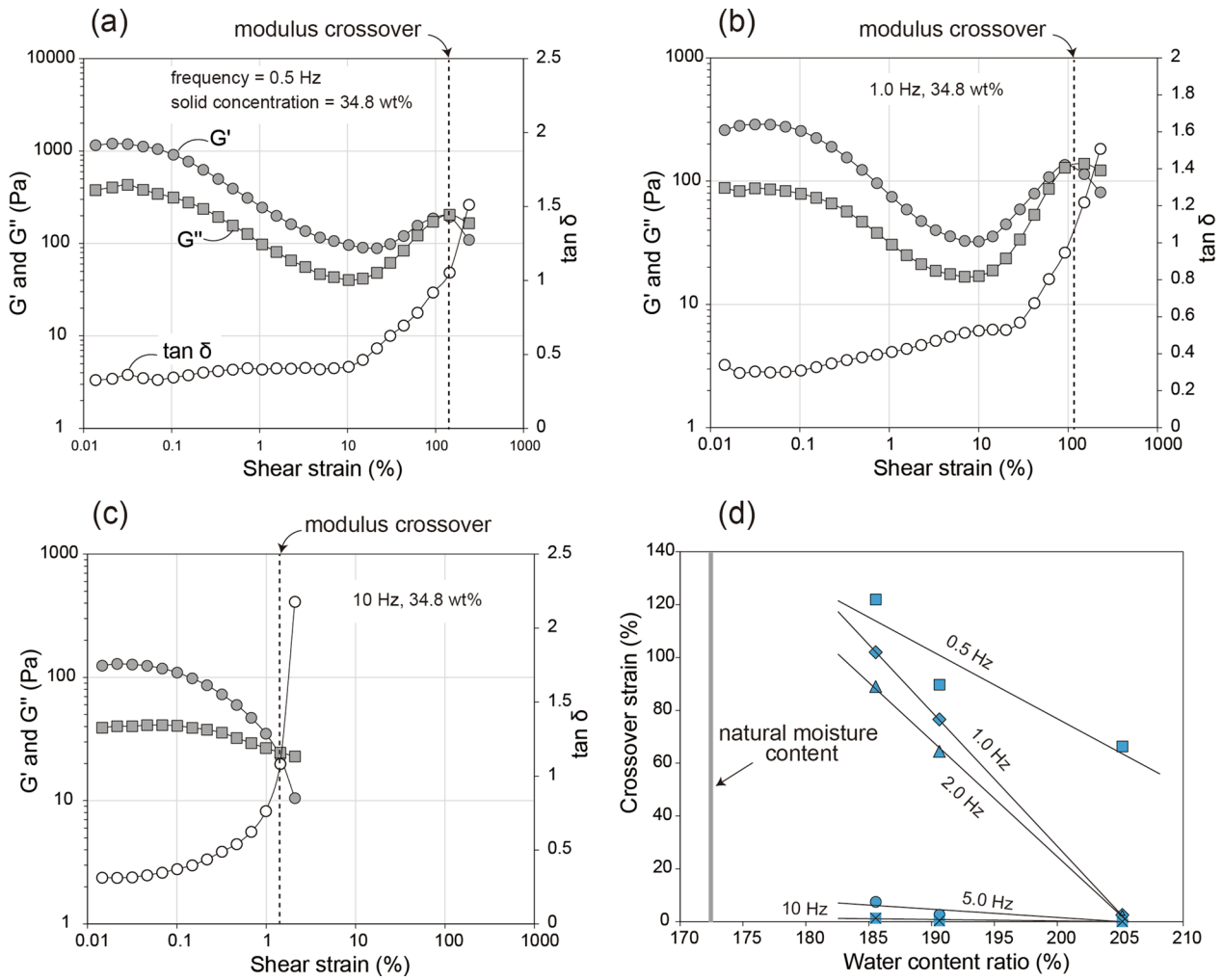

Fig. 8 (a–c) G', G'', and tan δ of slurry of moist soil with respect to shear strain at a solid concentration of 34.8 wt% with oscillatory frequency of **a** 0.5, **b** 1.0, and **c** 10 Hz. The crossover strain decreases with increasing frequency. **d** Summary of the crossover strain for each frequency with respect to water content. Natural moisture content is also shown

for constructing the empirical curves was determined by a dynamic method, i.e., interpolation of a stress–strain rate curve to obtain a shear stress in the limit of zero shear rate, which is commonly higher than the yield stress determined by the static and direct method adopted here.

Creep tests by Carrière et al. (2018) on several clay soils at different I_L states determined the critical shear stress at which the slurry viscosity bifurcates with increase of strain. Despite the clay slurries being prepared with dried samples, the stress values agreed well with the empirical relationship described above. Therefore, the low stress values obtained in this study may reflect the characteristics of the present sample, not the experimental method or sample preparation procedure.

An important finding of the present experiment is that the rheological properties of the slurry differ significantly between two different preparation methods (i.e., using dried or moist soil). Several studies have shown that the material properties of soils are altered by heating and drying (Casagrande 1932; Terzaghi et al. 1996; Huvaj and Uyeturk 2018). In general, after oven drying, the Atterberg limits such as liquid limit and plastic limit decrease by several tens of percent. Huvaj and Uyeturk (2018) studied the effect of drying on the Atterberg limit of pyroclastic soils containing halloysite, finding that the limits of samples dried at 60 °C or 110 °C were 1% to 30% lower than those of moist samples; they considered this likely owing to aggregation of the soil fabric or irreversible changes in the properties of halloysite after

drying. Figure 5a shows a difference of approximately 0.03 to 0.04 in the scale of ϕ for similar yield stress values between the two slurries, corresponding to a difference of ~ 40% of the water content ratio. This is equivalent to a ~ 20% decrease in water content (as a proportion of the total moisture content), which is roughly consistent with the findings of Huvaj and Uyeturk (2018). Such differences led the estimated yield stress of the two slurries at the natural moisture state to vary by several orders of magnitude, from 2.2 kPa to several pascals. Kameda and Okamoto (2021) assumed Bingham flow in a numerical model of a landslide triggered by the Eastern Iburi earthquake. The modeling constrained the yield stress of the collapsed soils in a saturated state to be ~ 1.5 kPa, which is of the same order as that of the slurry containing moist soil (i.e., 2.2 kPa), suggesting that such slurry is more likely to represent the soil state when the landslide occurred. In fact, in situ monitoring of the tephra after the earthquake indicated sustained high saturation (> 90%) even during a period of no precipitation (Wang et al. 2021). Similar tephra containing halloysite is likely to be widely distributed in volcanic regions worldwide. If it is sufficiently dried to the extent of the dried soil used in this study and then saturated by rainfall, its yield stress may be reduced significantly, as demonstrated in Fig. 4. It is also expected that the soil strength in such a state will decrease with time rather than immediately after hydration; therefore, these cases will show a time difference between precipitation and the onset of coseismic ground motion due to an earthquake, which will be an important factor in determining slope stability during the earthquake.

Dependence of slurry properties on pH

Our results demonstrate a dependence of yield stress on slurry pH at a given water content. Although the two types of slurry showed differing sensitivity to pH, the yield stress generally decreased under alkaline conditions and increased under acidic conditions (Fig. 6a), as predicted previously from measurements of zeta potential for samples with a finer size fraction (Kameda 2021). Comparison of the two types of slurry showed slurry made of dried soil had a more moderate dependence on pH than that made of moist soil. Zeta potential measurements in the present study used samples of the same size fraction as those used for the rheological tests; the potential showed a near-steady increase from a large negative value (− 40 mV) to near-zero with decreasing pH (Fig. 6b). A large negative zeta potential can enhance colloidal stability, and thus reduce the shear strength of slurry (Plaza et al. 2018). More quantitatively, the following model of yield stress–DLVO (Derjaguin–Landau–Verwey–Overbeeck) force and interaction energy have often been applied to clay slurries based on a constant surface potential for interactions between spherical particles (Scales et al. 1998):

$$\tau_y \approx \frac{\phi^2}{a}\left(\frac{A}{12{D_0}^2} - 2\pi\zeta^2\frac{\kappa e^{-\kappa D_0}}{1+e^{-\kappa D_0}}\right), \tag{6}$$

where a is the particle radius, A is the Hamaker constant, D_0 is the surface separation distance between interacting particles, and κ is the reciprocal of the Debye length (double-layer thickness). This model predicts a linear correlation between the yield stress and the square of zeta potential, and some clay slurries have been found to follow this correlation over a wide pH range (e.g., Au et al. 2014; Au and Leong 2016). As mentioned above, data for the slurry of dried soil show an almost linear correlation between yield stress and the square of zeta potential (Fig. 6c), indicating that the above yield stress–DLVO force model is likely applicable to the pH range tested here. In contrast, the results for the slurry of moist soil did not easily fit a single straight line. This may indicate either a change in the configuration of individual clay particles at different pH conditions (Shankar et al. 2010) or the addition of another attractive force, especially under acidic conditions, where the yield stress increased dramatically (Fig. 6a).

Although the microstructural mechanism for such behavior remains uncertain, the observed pH dependence of yield stress confirmed the prediction of Kameda (2021). Based on a simple mixing experiment of rainwater and tephra sample, Kameda (2021) raised the possibility of a change in pH of pore fluid in the tephra layer during rainfall, with pH likely increasing as the solid/liquid ratio decreases. If so, the chemical environment may have changed due to the rainfall before the earthquake in the present case, reducing the yield stress and thus the stability of the slope, which may have been a factor contributing to slope failure during the earthquake.

Fluidization of slurry under oscillatory strain

At the time of the Eastern Iburi earthquake, the slope was subjected to strong shaking with a maximum seismic intensity of 7 (JMA intensity scale) near the epicenter, which is thought to have directly triggered the slope collapse. To examine the effect of such periodic strain acting on the slope's weathered tephra, dynamic viscoelasticity tests were conducted at frequencies of 0.5 to 10 Hz (Figs. 7 and 8). The results indicate that both types of initially solid-like slurry can liquify within the tested frequency range. However, the slurry of moist soil had a higher resistance to oscillatory strain than the other slurry, as expected from the vane test, and its fluidizing

point occurred at a higher moisture content than in the case of the slurry of dried soil (Figs. 7d and 8d). In all cases, the strain amplitude of the solid–liquid transition (i.e., crossover strain) increased as the water content decreased or the frequency decreased. The slurry of moist soil, which is probably closer to the state of the soil at the time of the earthquake, had its crossover strain greatly increase when the applied frequency was less than 2 Hz, which may have been caused by the increase of storage modulus G' above a shear strain of ~ 10% (Fig. 8a, b). In this study, experiments at even lower ratios of water content, such as the natural moisture state, could not be performed, because the samples cracked during shearing. However, extrapolation of the experimental data indicates that the phase transition is expected under conditions of natural water content at small strain conditions when the frequency exceeds 5 Hz (Fig. 8d).

Previous geotechnical experiments using the same tephra materials indicated that halloysite-bearing tephra is more susceptible to liquefaction than other horizons under cyclic loading at a frequency of 1.5 Hz (Li et al. 2020). On the other hand, ground motion with strain occurring in several pulses at higher frequency (~ 3 Hz or more) during the earthquake was recorded at several seismological stations near the epicenter (Wang et al. 2019). Recent continuous seismic observation after the Eastern Iburi earthquake revealed that the characteristic frequency of the slope oscillation associated with seismic activity ranged between 5 and 7 Hz (Wang et al. 2020). The experimental results indicate that such oscillatory strain could easily fluidize the tephra layer, while at lower frequencies it may exhibit some resistance to fluidization. Although this study tested sieved soil whose original texture was completely broken, the obtained rheological properties may be a key to understanding the factors contributing to the stability of the slope during the long period after tephra deposition and the mechanism of eventual collapse due to seismic shaking.

Conclusions

This study investigated the rheological properties of weathered tephra slurry containing halloysite to understand the mechanical state of volcaniclastic soils during slope failure induced by the 2018 Hokkaido Eastern Iburi earthquake. The present experiments showed that the yielding and fluidizing behaviors of slurries depended on several factors, such as the water content, slurry pH, and frequency or amplitude of oscillatory strain. Furthermore, the method of preparing the tephra sample (i.e., complete drying versus retaining moisture) significantly influenced the rheological properties of the resulting slurry, with the slurry of moist soil apparently more closely reflecting the actual state of the soil when failure occurred. The slurry is expected to exhibit a yield stress of 2.2 kPa at its natural moisture content, in line with previous numerical modeling. The slurry's properties strongly depended on pH, suggesting that the actual mechanical state of the soil may change significantly in response to changes in the subsurface chemical environment. Dynamic viscoelasticity tests indicated that the slurry's resistance to fluidization under oscillatory shear strain could be greatly influenced by the frequency of the applied strain, with fluidization occurring at a relatively small strain amplitude, particularly when the applied cyclic strain is 5 Hz or higher. These results suggest the importance of evaluating the vibration characteristics of slopes during earthquakes and continuous observation of subsurface moisture state during and after rainfall, which is already being done by several research institutes. Additional monitoring of the subsurface chemical condition is also shown to be important. Such observational studies would be important in conducting risk assessments in areas with similar soils to those of the present study.

Supplementary Information

The online version contains supplementary material available at https://doi.org/10.1186/s40623-022-01623-4.

Additional file 1: Table S1. Summary of the measurement conditions and results for the vane tests. **Table S2.** Summary of the measurement conditions and results for the dynamic viscoelasticity tests.

Acknowledgements
I thank Tomonori Morisaki for technical assistance with the rheological experiment. I also acknowledge two anonymous reviewers and the editors A. Kato and I. Katayama for their constructive comments, which greatly improved the manuscript.

Author contributions
JK designed the study, carried out the experimental study, analyzed the data and construct manuscript. The author read and approved the final manuscript.

Funding
This work was supported by a JSPS Grant-in-Aid for Scientific Research (18H01295).

Availability of data and materials
The data sets supporting the conclusions of this article are included within the article.

Declarations

Competing interests
The author declare that they have no competing interest.

Received: 13 January 2022 Accepted: 4 April 2022
Published online: 11 May 2022

References

ASTM Standard D5311 (2011) Standard Test Method for Load Controlled Cyclic Triaxial Strength of Soil. ASTM International, West Conshohocken, PA.

Au PI, Siow SY, Avadiar L, Lee EM, Leong YK (2014) Muscovite mica and kaolin slurries: Yield stress–volume fraction and deflocculation point zeta potential comparison. Powder Technol 262:124–130

Au PI, Leong YK (2016) Surface chemistry and rheology of slurries of kaolinite and montmorillonite from different sources. KONA 33:17–32

Barnes HA, Hutton JF, Walters K (1989) An Introduction to Rheology. Elsevier Science Publishers, Amsterdam, The Netherland

Carrière SR, Jongmans D, Chambon G, Bièvre G, Lanson B, Bertello L, Berti M, Jaboyedoff M, Malet JP, Chambers JE (2018) Rheological properties of clayey soils originating from flow-like landslides. Landslides 15:1615–1630. https://doi.org/10.1007/s10346-018-0972-6

Casagrande A (1932) Research on the Atterberg limits of soils. Public Roads 13:121–136

Chigira M, Tajika J, Ishimaru S (2019) Landslides of pyroclastic fall deposits induced by the 2018 Eastern Iburi Earthquake with special reference to the weathering of pyroclastics. DPRI Annuals 62:348–356

Earthquake and Volcano Hazards Observation and Research Program (2019) Annual report. http://www.eri.u-tokyo.ac.jp/YOTlKYO/r1seikahoukoku/r1_kadai_seika_small.pdf

Geospatial Information Authority of Japan (2018) https://maps.gsi.go.jp/#12/42.770442/141.985660/&base=std&ls=std%7C20180906hokkaido_atsuma_0906do%7Cexperimental_anno&blend=0&disp=111&lcd=20180906hokkaido_atsuma_0906do&vs=c1j0h0k0l0u0t0z0r0s0m0f1&d=vl

Goh R, Leong YK, Lehane B (2011) Bentonite slurries–zeta potential, yield stress, adsorbed additives and time-dependent behavior. Rheol Acta 50:29–39

Huang W, Leong KY, Chen T, Au PI, Liu X, Qiu Z (2016) Surface chemistry and rheological properties of API bentonite drilling fluid: pH effect, yield stress, zeta potential and ageing behaviour. J Petrol Sci Eng 146:561–569

Huvaj N, Uyeturk E (2018) Effects of drying on Atterberg limits of pyroclastic soils of Northern Turkey. App Clay Sci 162:46–56. https://doi.org/10.1016/j.clay.2018.05.020

Ito Y, Yamazaki S, Kurahashi T (2020) Geological features of landslides caused by the 2018 Hokkaido Eastern Iburi Earthquake in Japan. Geol Soc London Spec Publ. https://doi.org/10.1144/SP501-2019-122

Jeong SW, Locat J, Leroueil S, Malet JP (2010) Rheological properties of fine-grained sediment: the roles of texture and mineralogy. Can Geotech J 47:1085–1100. https://doi.org/10.1139/T10-012

Joussein E, Petit S, Churchman J, Theng B, Righ D, Delvaux B (2005) Halloysite clay minerals: a review. Clay Miner 40:383–426

Kameda J, Kamiya H, Masumoto H, Morisaki T, Hiratsuka T, Inaoi C (2019) Fluidized landslides triggered by the liquefaction of subsurface volcanic deposits during the 2018 Iburi-Tobu earthquake, Hokkaido. Sci Rep 9:13119. https://doi.org/10.1038/s41598-019-48820-y

Kameda J (2021) Mineralogical and physico-chemical properties of halloysite-bearing slip surface material from a landslide during the 2018 Eastern Iburi earthquake, Hokkaido. Prog Earth Planet Sci 8:37. https://doi.org/10.1186/s40645-021-00428-5

Kameda J, Hamada Y (2021) Influence of biopolymers on the rheological properties of seafloor sediments and the runout behavior of submarine debris flows. Sci Rep 11:1493. https://doi.org/10.1038/s41598-021-81186-8

Kameda J, Okamoto A (2021) 1-D inversion analysis of a shallow landslide triggered by the 2018 Eastern Iburi earthquake in Hokkaido Japan. Earth Planets Space 73:116. https://doi.org/10.1186/s40623-021-01443-y

Kasai M, Yamada T (2019) Topographic effects on frequency-size distribution of landslides triggered by the Hokkaido Eastern Iburi Earthquake in 2018. Earth Planets Space 71:89. https://doi.org/10.1186/s40623-019-1069-8

Kluger MO, Moon VG, Kreiter S, Lowe DJ, Churchman GJ, Hepp DA, Seibel D, Jorat ME, Mörz T (2017) A new attraction-detachment model for explaining flow sliding in clay-rich tephras. Geology 45:131–134

Li R, Wang F, Zhang S (2020) Controlling role of Ta-d pumice on the coseismic landslides triggered by 2018 Hokkaido Eastern Iburi Earthquake. Landslides 17:1233–1250. https://doi.org/10.1007/s10346-020-01349-y

Locat J (1997) Normalized rheological behavior of fine muds and their flow properties in a pseudoplastic regime, Debris-flow hazards mitigation: mechanics prediction and assessment, Water Resources Engineering Division. Am Soc Civil Eng 1:260–269

Malet JP, Maquaire O, Locat J, Remaitre A (2004) Assessing debris flow hazards associated with slow moving landslides: methodology and numerical analyses. Landslides 25(1):83–90. https://doi.org/10.1007/s10346-003-0005-x

Moon V (2016) Halloysite behaving badly: geomechanics and slope behaviour of halloysite rich soils. Clay Miner 51:517–528

Nguyen QD, Boger DV (1983) Yield stress measurement for concentrated suspensions. J Rheol 27:321–349

Osanai N, Yamada T, Hayashi S, Katsura S, Furuichi T, Yanai S, Murakami Y, Miyazaki T, Tanioka Y, Takiguchi S, Miyazaki M (2019) Characteristics of landslides caused by the 2018 Hokkaido Eastern Iburi Earthquake. Landslides 16:1517–1528. https://doi.org/10.1007/s10346-019-01206-7

Plaza I, Ontiveros-Ortega A, Calero J, Romero C (2018) A new approach to triggering mechanism of volcano landslides based on zeta potential and surface free energy balance. Geomorph 301:1–9

Scales PJ, Johnson SB, Healy TW, Kapur PC (1998) Shear yield stress of partially flocculated colloidal suspensions. AIChE J 44:538–544

Scotto di Santolo A, Pellegrino AM, Evangelista A (2010) Experimental study on the rheological behaviour of debris flow. Nat Hazards Earth Syst Sci 10:2507–2514

Shankar P, Teo J, Leong YK, Fourie A, Fahey M (2010) Adsorbed phosphate additives for interrogating the nature of interparticles forces in kaolin clay slurries via rheological yield stress. Adv Powder Technol 21:380–385

Smoluchowski MV (1921) Handbook of Electricity and Magnetism. Barth, Leipzig, p 366

Sunil BM, Krishnappa H (2012) Effect of drying on the index properties of lateritic soils. Geotech Geol Eng 30:869–879

Terzaghi K, Peck RB, Mesri G (1996) Soil Mechanics in Engineering Practice. John Wiley & Sons

Theng BKG, Wells N (1995) The flow characteristics of halloysite suspensions. Clay Miner 30:99–106

Wada K, Mizota C (1979) The Clay Science Society of Japan, 42 (In Japanese).

Wang FR, Fan XM, Yunus AP, Subramanian SS, Alonso-Rodriguez A, Dai LX, Xu Q, Huang RQ (2019) Coseismic landslides triggered by the 2018 Hokkaido, Japan (Mw 6.6), earthquake: spatial distribution, controlling factors, and possible failure mechanism. Landslide 16:1551–1566. https://doi.org/10.1007/s10346-019-01187-7

Wang G, Ma N, Doi I, Furuya G, Watanabe M, Ishimaru S, Koyasu H, Cai F, Uchimura T, Kimura T (2020) Characteristics of ground motion on slopes of the 2018 Hokkaido Eastern Iburi Earthquake area based on the observation of microtremors and aftershocks. DPRI Annual Meeting 2020(D30):20–21

Wang F, Zhang S, Li R, Zhou R, Auer A, Ohira H, Dai Z, Inui T (2021) Hydrated halloysite: the pesky stuff responsible for a cascade of landslides triggered by the 2018 Iburi earthquake, Japan. Landslides 18:2869–2880. https://doi.org/10.1007/s10346-021-01656-y

Yamagishi H, Yamazaki F (2018) Landslides by the 2018 Hokkaido Iburi-Tobu Earthquake on September 6. Landslides 15:2521–2524

Zhang S, Li R, Wang F, Lio A (2019) Characteristics of landslides triggered by the 2018 Hokkaido Eastern Iburi earthquake, Northern Japan. Landslides 16:1691–1708. https://doi.org/10.1007/s10346-019-01207-6

Publisher's Note